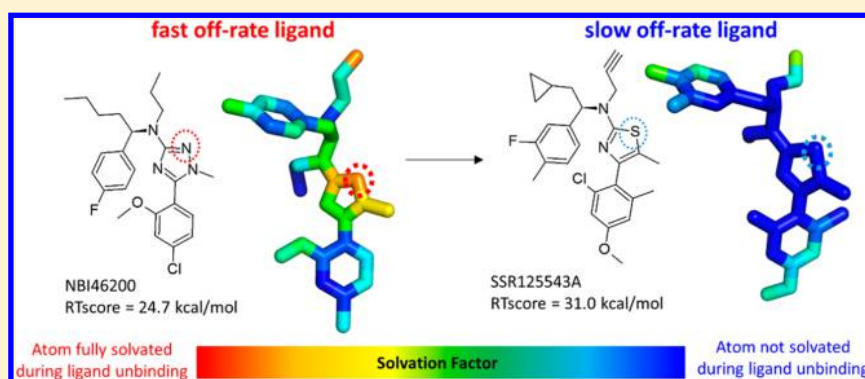


# Decoding the Role of Water Dynamics in Ligand–Protein Unbinding: CRF<sub>1</sub>R as a Test Case

Andrea Bortolato,<sup>\*,†</sup> Francesca Deflorian,<sup>†</sup> Dahlia R. Weiss, and Jonathan S. Mason

Heptares Therapeutics Ltd., BioPark, Broadwater Road, Welwyn Garden City, Hertfordshire AL7 3AX, U.K.

## S Supporting Information



**ABSTRACT:** The residence time of a ligand–protein complex is a crucial aspect in determining biological effect in vivo. Despite its importance, the prediction of ligand  $k_{\text{off}}$  still remains challenging for modern computational chemistry. We have developed aMetaD, a fast and generally applicable computational protocol to predict ligand–protein unbinding events using a molecular dynamics (MD) method based on adiabatic-bias MD and metadynamics. This physics-based, fully flexible, and pose-dependent ligand scoring function evaluates the maximum energy (RTscore) required to move the ligand from the bound-state energy basin to the next. Unbinding trajectories are automatically analyzed and translated into atomic solvation factor (SF) values representing the water dynamics during the unbinding event. This novel computational protocol was initially tested on two M<sub>3</sub> muscarinic receptor and two adenosine A<sub>2A</sub> receptor antagonists and then evaluated on a test set of 12 CRF<sub>1</sub>R ligands. The resulting RTscores were used successfully to classify ligands with different residence times. Additionally, the SF analysis was used to detect key differences in the degree of accessibility to water molecules during the predicted ligand unbinding events. The protocol provides actionable working hypotheses that are applicable in a drug discovery program for the rational optimization of ligand binding kinetics.

## INTRODUCTION

Transient formation of binary complexes between ligands and protein targets mediates many biochemical activities of cell physiology. The finite lifetimes of these interactions result in functional consequences that can be tightly regulated in terms of duration and amplitude of action.<sup>1</sup> Cell life depends ultimately on well-orchestrated receptor–ligand interactions where the longer the ligand is in residence at its receptor, the longer the biological effect endures. The residence time ( $\tau$ ), typically expressed as the inverse of the dissociation rate, can vary from milliseconds<sup>2</sup> to months,<sup>3</sup> but it is generally in the range of minutes or hours. The lifetime of the complex controls the effectiveness and duration of the biological action much more than the simple affinity of the ligand for its receptor. Tummino and Copeland<sup>1</sup> illustrated this concept in a very effective way by comparing the ligand–protein interaction to a violinist controlling the duration of a musical note by the length of time that the bow is drawn across a specific string.

Different studies have reported the importance of residence time to understand the activity of G protein-coupled receptor

(GPCR) ligands.<sup>4</sup> For example, slow dissociation increases the effect of angiotensin II AT<sub>1</sub> receptor antagonists.<sup>5</sup> Also, the residence times of M<sub>3</sub> muscarinic (M<sub>3</sub>) agonists are correlated with their intrinsic activities,<sup>6</sup> and slow dissociation of buprenorphine from the  $\mu$ -opioid receptor contributes to its pharmacodynamics in humans.<sup>7</sup> Ligand occupancy and residence time can also help to explain the difference between efficacy and toxicity. For example, the dopamine D<sub>2</sub> receptor antagonists haloperidol and chlorpromazine result in side effects that have been attenuated in more recent ligands with much shorter residence times.<sup>8,9</sup>

Despite its importance, ligand–protein residence time predictions still remain challenging for modern computational chemistry. In principle, all-atom molecular dynamics (MD) simulations should be able to address  $k_{\text{off}}$  evaluation, but they are limited by the time scales that can be routinely sampled (a few milliseconds), which are generally far shorter than ligand

Received: July 13, 2015

Published: September 3, 2015

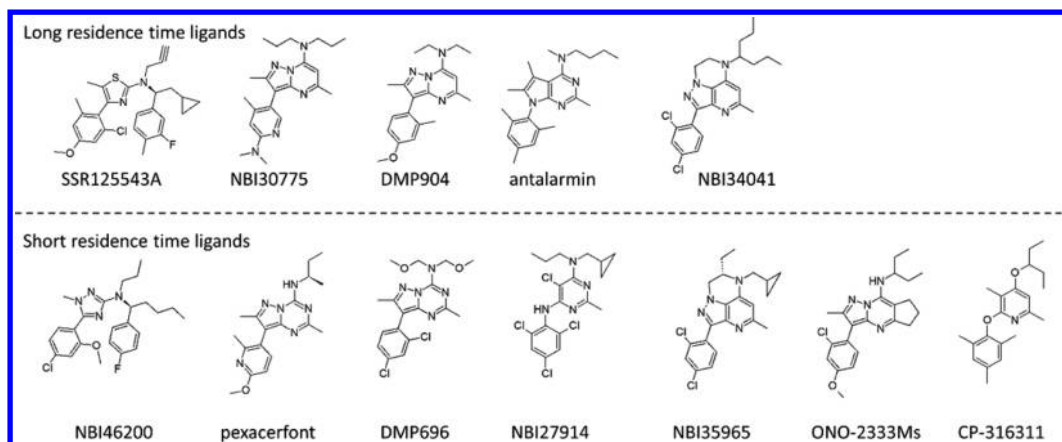


**Figure 1.** Chemical structures of the CRF<sub>1</sub> ligands considered in this study divided in two groups based on the residence time: long ( $\tau > 50$  min) and short ( $\tau < 20$  min).

dissociation time scales. This limit can be overcome by using enhanced sampling algorithms<sup>10</sup> such as metadynamics (MetaD) or by the construction of Markov state models (reviewed in refs 11 and 12, respectively). For example, recently the concept of “acceleration factor”<sup>13</sup> has been introduced to metadynamics<sup>14</sup> to study the ligand binding kinetics of the benzamide–trypsin complex with promising results. In parallel to these computationally demanding methods, fast approaches to evaluate the role of water molecules in affecting the ligand residence time have been proposed.<sup>15–17</sup> Schmidtke et al.<sup>15</sup> showed the importance of shielding hydrogen-bond (H-bond) interactions between the ligand and the protein from water molecules to increase the ligand unbinding transition state (TS) energy barrier. Pearlstein et al.<sup>16</sup> used WaterMap,<sup>18</sup> a method for predicting the preferred locations and thermodynamic properties of waters solvating proteins, to predict ligand  $k_{\text{on}}$  and  $k_{\text{off}}$ . They proposed that a fast on-rate can be related to replacement of protein H-bonds from waters to polar ligand atoms. Fast off-rates instead can be associated with limited displacement of unstable hydration sites. Trapped unstable waters between the protein and triazine antagonists were highlighted as important in limiting ligand residence times for the adenosine A<sub>2A</sub> receptor.<sup>17,19</sup>

We have developed a new computational chemistry protocol based on a combination of adiabatic-bias molecular dynamics (ABMD) and metadynamics to simulate ligand–protein unbinding events. The results provide a TS energy score (RTscore) that can be used to classify the residence times of ligands (fast vs slow off-rates) and provide insight into the water dynamics during ligand unbinding. This automatic method is simple to use, requiring only a starting protein–ligand complex and a target unbound ligand position. This aspect together with its speed (two ligands per day using 1 GPU) allows this approach to be applicable in the hit-to-lead and lead-optimization phases of drug development.

The novel method was initially tested on two M<sub>3</sub> and two adenosine A<sub>2A</sub> (A<sub>2A</sub>) antagonists with different residence times. The protocol was then used to evaluate 12 corticotropin-releasing factor receptor 1 (CRF<sub>1</sub>R) negative allosteric modulators (NAMs).<sup>20</sup> CRF<sub>1</sub>R is a class-B GPCR<sup>21</sup> activated by the corticotropin-releasing factor, a 41 amino acid peptide hormone with a key role in regulation of the stress response.<sup>22</sup> This receptor is implicated in pathophysiological conditions such as depression, post-traumatic stress disorder, and relapse in substance abuse. The 12 NAMs considered have similar

nanomolar binding affinities but different residence times (from less than 2 min to more than 7 h).<sup>20</sup> The ranking of dissociation half-lives of three of the ligands considered (NBI35965,  $t_{1/2} = 16$  min; NBI34041,  $t_{1/2} = 53$  min; NBI30775,  $t_{1/2} = 130$  min) is consistent with the ranking of their sustained suppression of adrenocorticotropin in vivo in adrenalectomized rats (NBI35965, <2 h; NBI34041, 4 h; NBI30775, 6 h). The fact that these three ligands have similar fast pharmacokinetics confirms that the sustained adrenocorticotropin suppression shown uniquely by NBI30775 is the result of its prolonged CRF<sub>1</sub>R occupancy.

## METHODS

**System Preparation.** The A<sub>2A</sub> crystal structure in complex with ligand 4e was downloaded from the Protein Data Bank<sup>23</sup> (PDB ID 3UZC).<sup>24</sup> Four of the stabilizing mutations were back-mutated to the wild-type residues (A107R, A202L, A235L, and A277S) to generate the same receptor used to evaluate the ligand residence time by Congreve et al.<sup>24</sup> The rotamer conformations of the side chains of these residues were modeled to be as similar as possible to the corresponding side chains in the crystal structure of A<sub>2A</sub> in complex with ZM241385 (PDB ID 4EII).<sup>25</sup> The receptor was prepared with the Protein Preparation Wizard in Maestro version 10.1 (Schrödinger, LLC, New York, NY, 2015): the H-bond network was optimized through an exhaustive sampling of hydroxyl and thiol moieties, tautomeric and ionic states of His, and 180° rotations of the terminal dihedral angles of amide groups of Asp and Gln. Hydrogen atoms were energy-minimized using the OPLS2.1 force field. Ligand 4a<sup>24</sup> was generated by modifying 4e in Maestro.

The human M<sub>3</sub> homology model in complex with tiotropium was generated in Prime version 3.9<sup>26</sup> (Schrödinger, LLC, New York, NY, 2015) using as a template the crystal structure of rat M<sub>3</sub> in complex with tiotropium (PDB ID 4U15).<sup>27</sup> The protein was prepared using the Preparation Wizard in Maestro as described above. Ipratropium was manually docked in Maestro using tiotropium as a reference and optimized using the refine protocol in Glide SP<sup>28</sup> (Glide, version 6.6; Schrödinger, LLC, New York, NY, 2015).

The basis for the simulations of the CRF<sub>1</sub>R NAMs was the crystal structure of CRF<sub>1</sub>R in complex with the small-molecule antagonist CP-376395 (PDB ID 4K5Y). As this structure contains some thermostabilizing mutations, we back-mutated

the residues to the wild-type sequence in silico. The homology model of wild-type CRF<sub>1</sub>R (from residue H117<sup>1,37</sup> to N367<sup>7,61</sup>; the superscripts show the Wooten numbering<sup>29</sup>) was generated using Prime version 3.9. The three-dimensional coordinates of CRF<sub>1</sub>R in complex with the small-molecule antagonist CP-376395<sup>30</sup> were used as a template. The receptor was prepared with the Protein Preparation Wizard in Maestro as described above. His155<sup>2,50</sup> was considered to be protonated. The ligands in Figure 1 were built and manually docked in the CP-376395 binding site in CRF<sub>1</sub>R using Maestro. The conformations were optimized using the refine protocol in Glide SP and SeeSAR version 2.2<sup>31</sup> (BioSolveIT, Sankt Augustin, Germany, 2015).

**Ligand–Protein Unbinding Prediction.** Ligand unbinding was predicted using aMetaD.py, a computational protocol written in Python based on open-source software: Gromacs v5.0.4,<sup>32</sup> Plumed v2.1.1,<sup>33</sup> and PyMol API. This automatic method requires the starting protein–ligand complex and a target unbound ligand position. No additional external user intervention is needed. For the A<sub>2A</sub> and M<sub>3</sub> ligands, the unbound conformations were generated by translating the bound ligands toward the extracellular side, above the extracellular loops at about 20 Å from the orthosteric site. For the CRF<sub>1</sub>R NAMs, unbound conformations were generated by positioning the ligand at about 20 Å from the bound state, into the membrane close to the extracellular portion of transmembrane helix 5 (TM5). This ligand unbinding direction resulted in the lowest energy barrier in a recent study of CP-376395 in CRF<sub>1</sub>R.<sup>34</sup>

The aMetaD.py protocol can be divided into two steps: (I) system preparation and equilibration; (II) adiabatic bias metadynamics (aMetaD). These steps are described below:

(I). **System Preparation and Equilibration.** The binding site, defined as a box with a distance from the ligand of 6 Å, was solvated using addWaters.py. This geometrical method (based on NumPy and SciPy) has been optimized to reproduce the water network around ligands in high-resolution GPCR crystal structures (data not shown). The AMBER99SB force field<sup>35</sup> parameters were used for the protein and the general Amber force field (GAFF)<sup>36</sup> for the ligands using AM1-BCC partial charges.<sup>37</sup> The system was embedded in a triclinic box including an equilibrated membrane consisting of 256 1,2-dimyristoyl-*sn*-glycero-3-phosphocholine (DMPC) lipids<sup>38</sup> and 24 513 waters using g\_membed<sup>39</sup> in Gromacs. The SPC water model was used, and ions were added to neutralize the system (final concentration 0.01M). An energy minimization protocol based on 1000 steps of the steepest-descent algorithm was applied to the system. The membrane was equilibrated by 0.5 ns of MD simulation with a time step of 2.5 fs using LINCS on all of the bonds and keeping the protein and ligand restrained by applying a force of 100 kJ mol<sup>−1</sup> nm<sup>−1</sup>. Lennard-Jones and Coulomb interactions were treated with a cutoff of 1.069 nm using particle-mesh Ewald (PME) electrostatics.<sup>40</sup> The MD simulation was executed in the NPT ensemble using v-rescale<sup>41</sup> (tau<sub>t</sub> = 0.5 ps) for the temperature coupling to maintain a temperature of 298 K and using Parrinello–Rahman<sup>42</sup> (tau<sub>p</sub> = 10.0 ps) for the semi-isotropic pressure coupling to maintain a pressure of 1.013 bar. Without application of any positional restraints, the system was minimized for 200 steps using the steepest-descent algorithm and equilibrated by MD using the same settings as described above but with a time step of 0.2 fs and increasing the temperature from 29.8 K to 298 K in 10 steps (nine steps of 30 ps and the last one of 300 ps).

(II). **Adiabatic-Bias Metadynamics (aMetaD).** The ligand unbinding event is predicted using a bias MD protocol based on a combination of adiabatic-bias MD<sup>43</sup> and well-tempered metadynamics.<sup>44</sup> ABMD applies a harmonic potential barrier only when the ligand is not moving toward a provided unbound reference location. It therefore allows exploration during the MD simulation of only ligand positions compatible with the small-molecule unbinding event. At the same time, the energy barrier to start the unbinding event is estimated using the metadynamics approach. In a metadynamics simulation, a history-dependent bias is added to the potential energy landscape. When this energy bias fills the bound-state energy basin, the ligand will move toward the unbound reference position, reaching the next closer energy well. In the ABMD, we define the quantity  $X^{(R,t)}$  as

$$X^{(R,t)} = d_{\text{TM}}(R(t), R^{\text{T}}) - \min_{t' \leq t} d_{\text{TM}}(R(t'), R^{\text{T}}) \quad (1)$$

where  $R(t)$  is the conformation of the ligand at time  $t$  during the simulation,  $R^{\text{T}}$  is the provided target ligand unbound conformation, and  $d_{\text{TM}}(R(t), R^{\text{T}})$  indicates the root-mean-square deviation (RMSD) of the ligand heavy atoms between the two positions. Thus,  $X$  is positive if the conformation  $R(t)$  is farther away from the target than the closest structure sampled at time  $t$ . To drive the system toward the ligand unbound target conformation  $R^{\text{T}}$ , we apply the following time-dependent bias potential:

$$U(R, t) = kH(X^{(R,t)})(X^{(R,t)})^2 \quad (2)$$

where  $H$  is the Heaviside function and  $k$  is an elastic constant. According to eq 2, the bias acts only when  $X$  is positive, i.e., when the ligand RMSD from the unbound conformation exceeds the minimum value achieved during simulation.

For the metadynamics, a generic path collective variable (CV)<sup>45</sup> is generated using the RMSD between the starting ligand bound state and a ligand position corresponding to the original starting ligand location translated by 3 Å on the  $X$  axis. Two path CVs are considered: one defining the RMSD position on this path ( $s$ ) and the other the RMSD distance from the path ( $z$ ). In the well-tempered metadynamics simulations,<sup>44</sup> a history-dependent bias composed of intermittently added Gaussian functions is included in the potential. The bias is updated by adding Gaussian contributions with a total height of

$$W = W_0 \exp\left(-\frac{V_i(s, z)}{fT}\right) \quad (3)$$

where  $W_0$  is the initial Gaussian height,  $T$  is the simulation temperature,  $f$  is the bias factor, and  $V_i(s, z)$  is the bias potential at time  $t$  for the values  $s$  and  $z$  of the CVs.

The ligand unbinding path was generated with 300 ps of aMetaD using the same MD settings as in the final system equilibration at 298 K. For the adiabatic-bias MD,<sup>43</sup> the target ligand position was correctly aligned to the new equilibrated system using the PyMol API. A force constant of 150 kJ mol<sup>−1</sup> nm<sup>−2</sup> and a target RMSD of 0.001 nm with respect to the unbound ligand conformation were applied. ABMD was combined with the well-tempered metadynamics simulation<sup>44</sup> with the following settings: a simulation temperature of 298 K, a bias factor of 3300, and an initial energy bias Gaussian height of 0.5 kcal/mol with a deposition frequency of 0.5 ps. The width of the Gaussians was 0.05 Å. Recently, similar



metadynamics parameters were used to predict ligand–protein unbinding on a different system.<sup>14</sup>

**RTscore and Solvation Factor.** For every ligand, the aMetaD.py protocol performs four independent replicas. Each replica is composed of one repetition of step I (system preparation and equilibration) followed by three independent repetitions of step II (aMetaD). Therefore, for every ligand this protocol simulates a total of 12 unbinding events, requiring in total about 12 h on a single computer with 1 GPU (GTX980 or GTX780) and 6 CPU cores (Intel i7@3.4 GHz). In a recent study, 12 independent metadynamics runs were sufficient to obtain a reliable estimate of the ligand  $k_{\text{off}}$ .<sup>14</sup> The simulation of 12 unbinding events for every ligand using the aMetaD approach resulted in converged frequencies of long and short residence time predictions (Figures S1 and S2) and average RTscore (Figure S3).

We suppose that the ligand bound state is located in a low-energy basin on the free energy hypersurface representing the ligand unbinding event that is separated by a transition state (or dynamical bottleneck) from a second basin. We assume that the time taken to cross this bottleneck is much less than the time spent in the individual basins.<sup>46</sup> During the aMetaD protocol, the metadynamics run accumulates bias against visited states and gradually enhances the probability of visiting different energy basins without depositing bias near the TS. On the basis of these assumptions, we can define the metadynamics acceleration factor  $\alpha$  as<sup>47</sup>

$$\alpha(t) = \langle e^{\beta V(s(R),t)} \rangle_M \quad (4)$$

where the angle brackets denote an average over a metadynamics run confined to a particular energy basin  $M$ ,  $V(s, t)$  is the metadynamics time-dependent bias, and  $\beta = (k_B T)^{-1}$ , where  $k_B$  is the Boltzmann constant.

For every unbinding event, we recorded the following data every 0.2 ps in the COLVAR file: (1) the energy bias  $V$  (resulting from the metadynamics algorithm) that the ligand is experiencing and (2) the metadynamics acceleration factor  $\alpha$ .<sup>47</sup> In the aMetaD method, we assumed that the ligand reached a new energy basin ( $M'$ ) when  $\alpha$  did not increase more than 2-fold for at least 100 ps. On this basis, we calculated the residence time score (RTscore) as

$$\text{RTscore} = \max(V(s(R), t)_{M_0}) \quad (5)$$

The RTscore is therefore the maximum energy bias that the ligand experienced before a transition from the starting ligand bound state ( $M_0$ ) to another energy basin.

For every ligand, 192 snapshots ( $n$ ) from the 12 predicted unbinding events were used to evaluate the solvation factor (SF) for the complex. For every protein–ligand heavy atom ( $a$ ), we define the SF as

$$\text{SF}(a) = \sum_1^n \text{sf}(a, O) \quad (6)$$

where  $\text{sf}(a, O)$  is different from zero and equal to 0.5 only if atom  $a$  has at least one water oxygen at a distance of less than 4 Å in the particular MD snapshot considered. Therefore, the SF for each atom is a number in the range from 0 (atom never solvated during ligand unbinding) to 96 (atom always solvated during ligand unbinding). For easy visualization, SFs are stored in the PDB B Factor column of the original input protein–ligand complex.

## RESULTS AND DISCUSSION

**RTscore.** In contrast to predictions based on equilibrium free energy of binding, nonequilibrium kinetics cannot be simplified as a simple two-state model corresponding to the ligand–protein bound and unbound conformations. A very high number of different ligand unbinding paths are possible, with unique energy profiles and different occurrence probabilities, leading to a highly multidimensional free energy landscape. To try to address the complexity of the ligand kinetics, we simulate the unbinding event for every ligand 12 times as a reasonable compromise between speed and accuracy (Figures S1–S3). The computational approach is indeed fast enough to be suitable in the hit-to-lead and lead-optimization stages. At the same time, it is precise enough to obtain a useful discrimination of ligands with about half an hour difference in residence time between them.

Every ligand unbinding event is predicted using aMetaD, a new computational protocol employing biased MD. This approach is based on the combination of ABMD and metadynamics:

1. ABMD applies a harmonic potential that is zero when the ligand is moving toward a provided unbound reference location and stops the ligand if it attempts to move in the opposite direction. ABMD therefore allows exploration during the MD simulation of only ligand positions compatible with the small-molecule unbinding event.
2. The energy barrier to start the unbinding event is estimated by applying a metadynamics algorithm in parallel with the described ABMD. In a metadynamics simulation, a history-dependent bias is added to the potential energy landscape. When this energy bias fills the bound-state energy basin, the ligand will move toward the unbound reference position, reaching the next closer energy well.

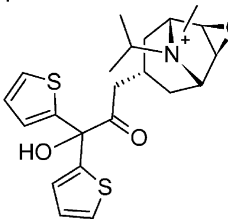
In particular, the method has been developed to be easy to use, fast, and widely applicable. This automatic protocol does not require external user intervention beyond the input docked ligand pose and a target unbound position. At the same time, the details of every step of the calculations are reported. Additionally, the final results (RTscore and solvation factor, described below) do not require expert knowledge to be analyzed. Thanks to the addition of ABMD to the MetaD, the protocol is fast enough to evaluate two ligands a day on a desktop computer with a modern GPU card. Finally, aMetaD is widely applicable, thanks to the use of a generic path CV for the MetaD that does not require specific testing or optimization.

Despite the use of metadynamics as a core approach, aMetaD is unable to evaluate the precise energy landscape of the ligand unbinding event or to detect the exact energy barrier dividing the bound and unbound states. This protocol is instead a physics-based, fully flexible, and pose-dependent ligand scoring function. It uses an energy bias to break ligand–protein interactions and to promote the start of the unbinding event. For every unbinding event, it provides a residence time score (RTscore) based on the maximum energy (TS energy) required to move the ligand from the starting energy basin to the next. In cases where the start of the ligand unbinding event represents an important kinetic bottleneck, the RTscore is assumed to be related to the ligand residence time. We initially tested this hypothesis on two Family A GPCRs: the  $A_{2A}$  and  $M_3$  receptors. For both systems, we selected two ligands with

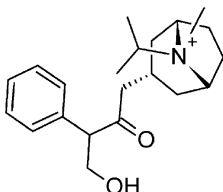
Table 1. Summary of the RTscore Predictions (Runs 1–12) and Experimental Binding Residence Times for the M<sub>3</sub> and A<sub>2A</sub> Ligands<sup>a</sup>

		M <sub>3</sub>		A <sub>2A</sub>	
		tiotropium	ipratropium	4e	4a
Residence time (min) <sup>24,48</sup>		>1440	17	16	<1
K <sub>i</sub> (nM) <sup>24,48</sup>		0.19	0.05	0.14	11.75
RTscore (kcal/mol)	run 1	22.2	24.5	18	16.7
	run 2	31.9	26.2	14.8	8.8
	run 3	38.3	18.2	21.1	14.2
	run 4	39.6	18.7	31	14.3
	run 5	33.9	33.3	16.9	16.8
	run 6	35.2	31.3	30.2	11.8
	run 7	34.9	22.5	15.3	11.5
	run 8	21.9	25.8	16.8	24.2
	run 9	22.5	22.3	34.9	27.2
	run 10	24.8	23.8	19	19.1
	run 11	30.7	27	19.3	17.1
	run 12	21.4	23.9	11.6	25.5
average		29.8	24.8	20.7	17.3
% RTscore > 30 kcal/mol (long residence time)		58.3	16.7	25	0
% RTscore < 20 kcal/mol (short residence time)		0	16.7	66.7	75

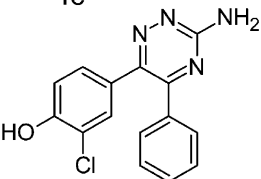
tiotropium



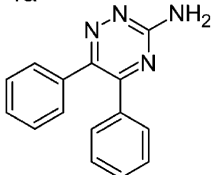
ipratropium



4e



4a



<sup>a</sup>The percent frequencies with which ligands are predicted to have a long (RTscore > 30 kcal/mol) or short (RTscore < 20 kcal/mol) residence times are shown. It should be noted that intermediate RTscores between 20 and 30 kcal/mol are not tallied, as they may lead to short or long residence times.

different residence times (Table 1): for A<sub>2A</sub>, 4a ( $\tau$  < 1 min) and 4e ( $\tau$  = 16 min);<sup>24</sup> for M<sub>3</sub>, tiotropium ( $\tau$  > 1440 min) and ipratropium ( $\tau$  = 17 min).<sup>48</sup> Crystal structures of the A<sub>2A</sub>–4e and M<sub>3</sub>–tiotropium complexes are available, allowing the generation of reliable starting binding modes for these four ligands. The average of the RTscores obtained from the 12 runs successfully discriminate the difference in residence times among the ligands (Table 1). The long-residence-time tiotropium was the only molecule predicted to result in a frequent (>50%) high-energy barrier for unbinding (RTscore > 30 kcal/mol).

We further evaluated aMetaD on a set of 12 small-molecule NAMs of CRF<sub>1</sub>R (Figure 1).<sup>20</sup> Regardless of similar low-nanomolar binding affinities, these structurally related molecules have residence times spanning from 2.6 to 430 min (Table 1). In particular, five of them have long residence times greater than 50 min. With the publicly available crystal structure of CRF<sub>1</sub>R in complex with a small NAM,<sup>30</sup> it has been possible to create reasonable starting docking solutions for these ligands to be used for the aMetaD protocol. It is important to note that the aMetaD predictions are affected by

the starting ligand docked pose. However, the initial MD-based system equilibration optimizes the starting protein–ligand complex using the same force field exploited for the following metadynamics-based scoring. For the target conformation that is used to drive the unbinding direction for the ABMD, we used a ligand position about 20 Å from the bound state in the membrane close to the extracellular portion of TM5. This ligand unbinding direction was shown to have the lowest energy barrier in a recent study for CP-376395 in CRF<sub>1</sub>R.<sup>34</sup> The resulting RTscores for the 12 runs are reported in Table 1. It is not possible to avoid or further decrease the RTscore variability for the different runs; this is a direct consequence of the diverse energy landscapes of the different ligand unbinding paths. However, the simulation of 12 unbinding events for every ligand resulted in converged residence time predictions (Figures S1–S3). We use the frequency with which a ligand is predicted to have a long (RTscore > 30 kcal/mol) or short (RTscore < 20 kcal/mol) residence time (Table 2) to discriminate long-acting ligands. Indeed, the five ligands with  $\tau$  > 50 min are predicted to have RTscore > 30 kcal/mol (long  $\tau$ ) in above 30% of the cases and RTscore < 20 kcal/mol (short

**Table 2.** Summary of the RTscore Predictions (Runs 1–12) and Experimental Binding Residence Times for the CRF<sub>1</sub>R Ligands<sup>a</sup>

	long-residence-time ligands					short-residence-time ligands						
	SSR125543A	NBI30775	DMP904	antalarmin	NBI34041	ONO-2333Ms	NBI35965	pexacerfont	DMP696	NBI46200	CP-316311	NBI27914
residence time (min) <sup>20</sup>	430	130	96	53	53	17	16	14	7.3	5.3	4.1	2.6
K <sub>i</sub> (nM) <sup>b,20</sup>	0.3	2.6	0.6	1.4	1.3	1.2	1.1	7.4	2.2	1.3	1.9	1.0
RTscore (kcal/mol)												
run 1	34.6	35.4	29.9	24.3	35.3	27.5	47.1	26.6	22.9	21.5	14.8	16.4
run 2	22.9	30.0	35.6	23.3	23.0	31.8	32.9	19.5	45.1	17.0	21.3	20.1
run 3	51.2	32.8	29.4	32.6	43.1	23.1	27.7	23.1	20.8	36.2	21.5	18.3
run 4	41.5	37.5	27.3	23.1	23.2	13.9	19.6	20.9	34.6	33.8	14.5	21.4
run 5	20.7	42.1	30.6	35.9	30.1	18.2	18.7	59.6	23.0	24.0	12.3	22.8
run 6	25.5	33.4	23.1	24.3	24.1	17.4	22.2	28.4	27.0	20.2	28.1	19.1
run 7	22.7	21.3	29.7	23.5	35.3	27.8	19.5	23.1	20.2	19.4	18.4	23.6
run 8	36.1	38.0	18.7	20.9	26.6	26.1	25.7	22.8	17.2	18.9	22.7	23.8
run 9	21.2	26.0	23.6	36.7	17.8	25.6	19.7	20.7	23.0	23.7	21.0	22.6
run 10	37.8	19.1	30.8	37.7	21.9	20.2	30.8	33.3	20.4	21.2	21.8	28.6
run 11	28.1	22.4	36.1	41.2	26.9	24.6	24.8	26.8	27.4	39.2	18.2	19.9
run 12	29.3	23.5	31.1	21.9	21.0	19.8	22.8	24.9	25.1	21.8	25.2	33.8
avg	31.0	30.1	28.8	28.8	27.4	23.0	26.0	27.5	25.6	24.7	20.0	22.5
% with RTscore > 30 kcal/mol (long residence time)	41.7	50.0	41.7	41.7	33.3	8.3	25.0	16.7	16.7	25.0	0.0	8.3
% with RTscore < 20 kcal/mol (short residence time)	0.0	8.3	8.3	0.0	8.3	33.3	33.3	8.3	8.3	25.0	41.7	33.3

<sup>a</sup>The percent frequencies with which ligands are predicted to have long (RTscore > 30 kcal/mol) or short (RTscore < 20 kcal/mol) residence times are shown. It should be noted that intermediate RTscores between 20 and 30 kcal/mol are not tallied, as they may lead to short or long residence times. <sup>b</sup>Competition assay vs <sup>125</sup>I-sauvagine.

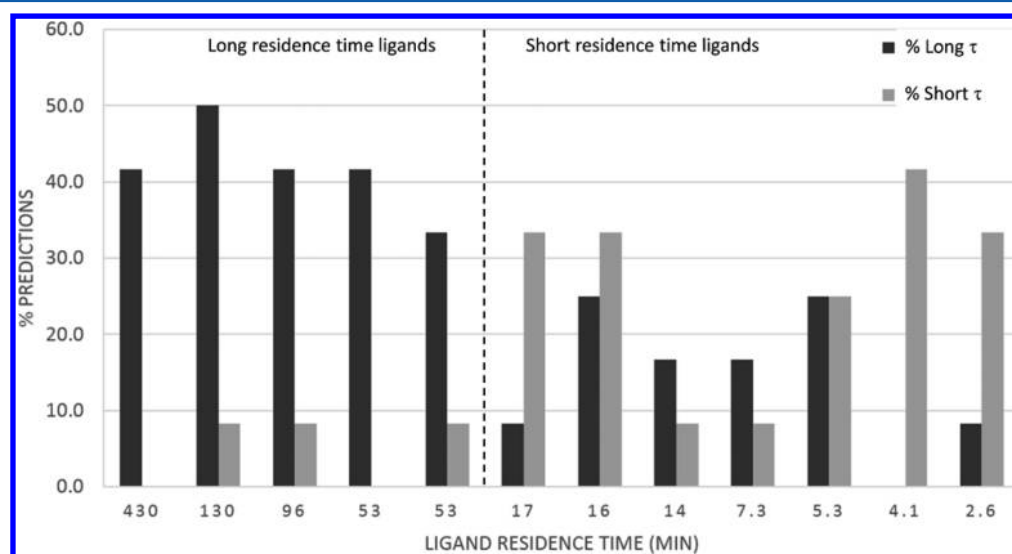


**Figure 2.** Histogram representation of the frequencies with which the CRF<sub>1</sub>R ligands were predicted by RTscore to have a long residence time (in black, RTscore > 30 kcal/mol) or a short residence time (in gray, RTscore < 20 kcal/mol). The experimental residence times of the ligands are reported on the X axis. Long ( $\tau > 50$  min) and short ( $\tau < 20$  min) residence time ligands are divided by the dashed line.

$\tau$ ) in less than 10% of the cases (Figure 2). The remaining seven ligands with faster off-rates are predicted to have a long  $\tau$  in less than 20% of the cases. It should be noted that simulations with RTscores between 20 and 30 kcal/mol were discarded, as that range proved to be not useful to discriminate changes in ligand residence time.

**Solvation Factor.** Solvation of the ligand and the protein binding site during the unbinding event can play a crucial role in determining the lifetime of the complex. To understand the

water dynamics upon unbinding, we developed a simple yet powerful way to analyze the 12 trajectories resulting from the aMetaD protocol for every ligand. Every trajectory is divided into 16 snapshots (resulting in a total of 192 snapshots). For every protein–ligand atom, the solvation factor (SF) is calculated as half of the number of times in these snapshots a given atom has at least one water at a distance of less than 4 Å. Therefore, the SF for each atom is a number from 0 (atom never solvated during ligand unbinding) to 96 (atom always

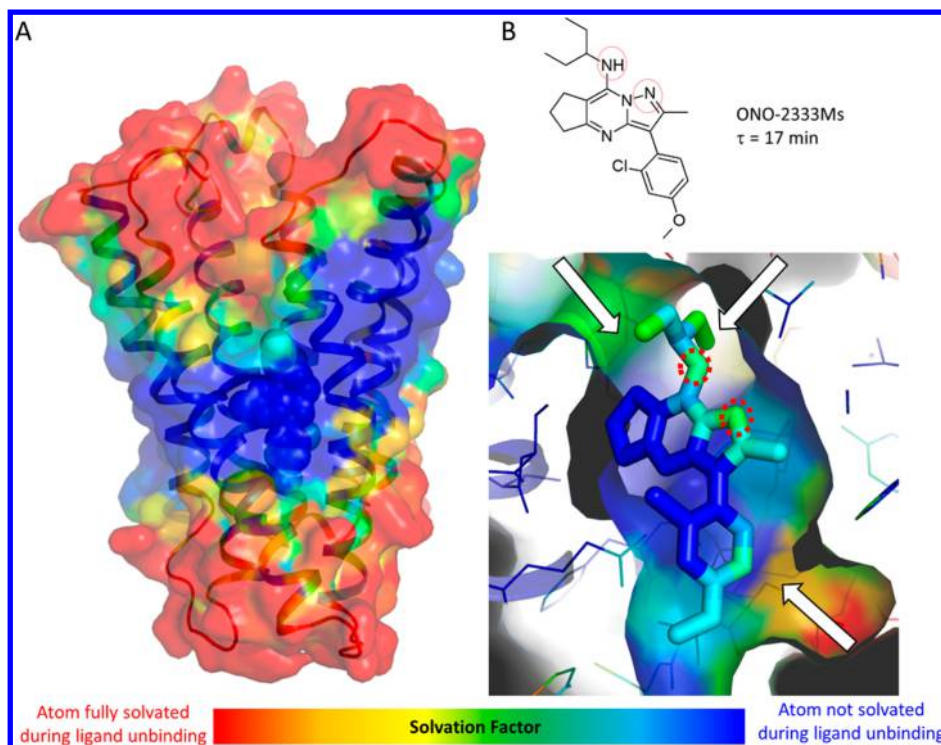


**Figure 3.** Solvation factor representation. (A) Starting conformation of the CRF<sub>1</sub> receptor (shown in the ribbon representation) in complex with NBI34041 (shown as spheres). The protein surface and the ligand are color-coded according to the solvation factor using rainbow colors from red (atom fully exposed to the waters during the ligand unbinding event) to blue (atom never in contact with the solvent during unbinding) as indicated in the bottom bar. (B) At the top, the 2D structure of ONO-2333Ms is shown. At the bottom, the 3D conformation of the ligand in complex with CRF<sub>1</sub>R is shown using the same coloring scheme as in (A). The protein backbone is shown in the ribbon representation and the binding site as a surface; ligands are shown as sticks and protein atoms as lines. Important atoms solvated during ligand unbinding are highlighted by dotted red circles. Arrows indicate regions of the ligand and the pocket that are at the interface with water molecules.

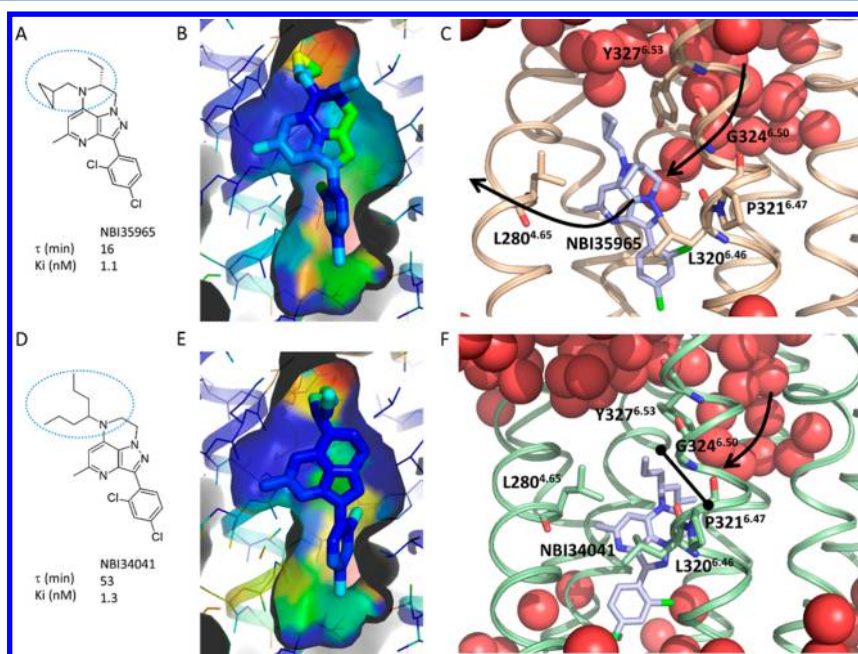


**Figure 4.** Comparison of the water dynamics difference between the fast-off-rate ligand NBI35965 (A–C) and the slow-off-rate ligand NBI34041 (D–F). In (A) and (D), dotted circles highlight the structural differences in the 2D structures of the small molecules. In (B) and (E), ligand bound states are shown color-coded according to the solvation factor as in Figure 3. The protein backbone is shown in the ribbon representation, while ligands are shown as sticks and protein atoms as lines. Representative conformations corresponding to the start of the unbinding for NBI35965 and NBI34041 are included in (C) and (F), respectively. The ligands and a few selected residues are shown as in the stick representation, and water molecules are shown as spheres. Arrows highlight the movement of the waters contributing to NBI35965 unbinding (C) and opposed by NBI34041 interactions with Y327<sup>6.53</sup> (F).



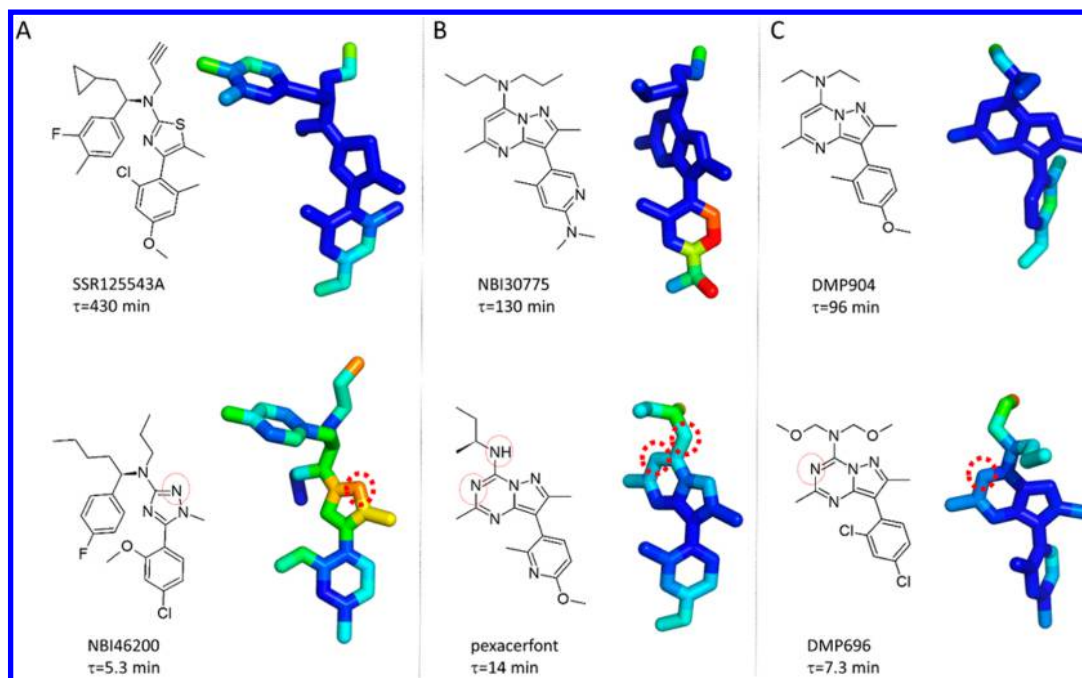


**Figure 5.** Comparison of solvation factors for structurally related ligand pairs with different residence times: (A) SSR125543A and NBI46200; (B) NBI30775 and pexacerfont; (C) DMP904 and DMP696. Every ligand is shown as a 2D structure and in the stick representation color-coded according to the solvation factor as in Figure 3. Important atoms solvated during ligand unbinding are highlighted by dotted red circles. Structurally related long- and short-residence-time ligands are shown in the top and bottom rows, respectively.

solvated during ligand unbinding). For easy visualization, SFs are stored in the PDB B Factor column of the original input protein–ligand complex and used to color-code the atoms as a rainbow from blue (SF = 0) to red (SF = 96).

The SF coloring scheme allows easy visualization of the degree of accessibility to water molecules during the predicted ligand unbinding events. For example, it is possible to visualize the irregular position of the membrane around the receptor helical bundle (Figure 3A). In particular, it is interesting to note the ability of water molecules to interact with the extracellular side of TM5 and TM6, reaching G274<sup>5,41</sup> and Y327<sup>6,53</sup> right above the NAM binding region. The same analysis of the NAM pocket and the ligand allows the movement of the solvent during ligand unbinding to be determined (Figure 3B). This highlights the key ligand atoms that are solvated, the direction from which the waters access the pocket, and which parts of the protein binding site are touched by waters and for how long. For example, for the ligand ONO-2333Ms, the secondary amino group and the pyrazole nitrogen are key polar atoms that are solvated during unbinding.

SF analysis is particularly interesting when comparing structurally related ligands with dissimilar residence times. For example, the only difference between NBI35965 and NBI34041 is the totally lipophilic alkyl substitutions in the nonaromatic top ring (6/7 carbon atoms, which increases  $\tau$  from 16 to 53 min (Figure 4A,D)). This structural change seems to have an important effect on the ligand solvation during unbinding: in NBI35965, waters access the pyrazole nitrogen (Figure 4B,C), whereas in NBI34041, the heptane chain substitution better interacts with Y327<sup>6,53</sup>, stopping the water flow in the pocket and contributing to a longer ligand residence time (Figure 4E,F).

Similarly, it is possible to detect key structural changes affecting ligand solvation in other ligand pairs sharing the same scaffold (Figure 5):

- (A) The change of the central polar triazole in NBI46200 to the more hydrophobic and bulkier thiazole in SSR125543A dramatically changes the ligand SF (Figure 5A). The nitrogen in position 2 of the triazole is solvated during the early stages of ligand unbinding and promotes the breaking of the protein–ligand interactions, which could explain the residence time difference between NBI46200 ( $\tau$  = 5.3 min) and SSR125543A ( $\tau$  = 430 min).
- (B) The hydrophobic tails of the NBI30775 tertiary amino group are effective in stopping the water flow from the extracellular side of the pocket (Figure 5B). Similarly, in the intracellular portion of the binding site the pyridine nitrogen creates a stable interface with the waters, contributing to the long residence time ( $\tau$  = 130 min). In contrast, pexacerfont is less effective in preventing water access to the binding site: its secondary amino group promotes solvation of the nitrogens in positions 3 and 6 of the pyrazoletriazine core, while to optimize its *o*-methyl hydrophobic interactions the pyridine is oriented with the nitrogen not facing the water interface.
- (C) Similar considerations apply for DMP904 ( $\tau$  = 96 min) and DMP696 ( $\tau$  = 7.3 min) (Figure 5C). The substitutions of the diethylamine group and pyrimidine ring in DMP904 with the more polar bis-(methoxymethyl)amine substituent and triazine ring, respectively, in DMP696 promote the solvation of the ligand and the pocket binding site, potentially increasing the small-molecule  $k_{\text{off}}$ .

## CONCLUSION

The residence time of a ligand–protein complex can be a crucial aspect in achieving a prolonged biological effect in vivo. Despite its importance, the prediction of ligand  $k_{\text{off}}$  still remains



challenging for modern computational chemistry. We have developed aMetaD, a new computational protocol to predict ligand–protein unbinding events using a MD method based on adiabatic-bias MD and metadynamics. The speed of this automatic approach (two ligands per day on a desktop computer with a modern GPU card) and its general applicability allow aMetaD to potentially be used routinely in drug discovery projects during the hit-to-lead and lead-optimization stages.

This novel protocol simulates a “stress test” on a ligand-docked solution. It provides an energy bias to break ligand–protein interactions and to promote the start of the unbinding event. This physics-based, fully flexible, and pose-dependent ligand scoring function evaluates the maximum energy (TS energy) required to move the ligand from the starting energy basin to the next. In an initial test, the aMetaD approach was able to discriminate differences in residence time in two couples of structurally related Family A GPCR ligands. On a set of 12 Family B CRF<sub>1</sub>R ligands, the resulting score (RTscore) was used successfully to categorize ligands with residence time differences above 30 min.

The unbinding trajectories are automatically analyzed and translated to atomic solvation factor (SF) values representing the water dynamics during the unbinding event. SFs are stored in the PDB B Factor field to be easily analyzed by any molecular modeling visualization software. The SF coloring scheme has been used to detect key differences in the degree of accessibility to water molecules during the predicted ligand unbinding events for the CRF<sub>1</sub>R NAM test set. This simple analysis provides examples of actionable working hypotheses applicable in a discovery program to rationally optimize ligand binding kinetics.

Although more tests are certainly needed to prove the general applicability of aMetaD, RTscore, and SF, the general concepts outlined here could be applied to other types of nonstandard MD methods for predicting ligand unbinding and binding events and could potentially provide a general framework of protocols usable in drug discovery projects to predict ligand kinetics.

## ■ ASSOCIATED CONTENT

### Supporting Information

The Supporting Information is available free of charge on the ACS Publications website at DOI: 10.1021/acs.jcim.5b00440.

Residence time and RTscore prediction convergence analysis (PDF)

## ■ AUTHOR INFORMATION

### Corresponding Author

\*Phone: +44(0)1707 358646. Fax: +44(0)1707 358640. E-mail: andrea.bortolato@heptares.com.

### Author Contributions

<sup>†</sup>A.B. and F.D. contributed equally to this work.

### Notes

The authors declare no competing financial interest.

## ■ ACKNOWLEDGMENTS

The authors thank Ben Tehan, Rob Cooke, and Fiona Marshall for useful discussions and critical reading of the manuscript.

## ■ REFERENCES

- (1) Tummino, P. J.; Copeland, R. A. Residence Time of Receptor–Ligand Complexes and Its Effect on Biological Function. *Biochemistry* **2008**, *47*, 5481–5492.
- (2) Hanahan, D.; Weinberg, R. A. Hallmarks of Cancer: the Next Generation. *Cell* **2011**, *144*, 646–674.
- (3) Gupta, P. B.; Mani, S.; Yang, J.; Hartwell, K.; Weinberg, R. A. The Evolving Portrait of Cancer Metastasis. *Cold Spring Harbor Symp. Quant. Biol.* **2005**, *70*, 291–297.
- (4) Guo, D.; Hillger, J. M.; IJzerman, A. P.; Heitman, L. H. Drug–Target Residence Time—a Case for G Protein-Coupled Receptors. *Med. Res. Rev.* **2014**, *34*, 856–892.
- (5) Verheijen, I.; Vanderheyden, P. M.; De Backer, J. P.; Vauquelin, G. AT1 Receptor Antagonists. *Curr. Med. Chem.: Cardiovasc. Hematol. Agents* **2004**, *2*, 69–77.
- (6) Dowling, M. R.; Charlton, S. J. Quantifying the Association and Dissociation Rates of Unlabelled Antagonists at the Muscarinic M3 Receptor. *Br. J. Pharmacol.* **2006**, *148*, 927–937.
- (7) Yassen, A.; Olofsen, E.; Romberg, R.; Sarton, E.; Danhof, M.; Dahan, A. Mechanism-Based Pharmacokinetic-Pharmacodynamic Modeling of the Antinociceptive Effect of Buprenorphine in Healthy Volunteers. *Anesthesiology* **2006**, *104*, 1232–1242.
- (8) Kapur, S.; Seeman, P. Antipsychotic Agents Differ in How Fast They Come Off the Dopamine D2 Receptors. Implications for Atypical Antipsychotic Action. *J. Psychiatry Neurosci.* **2000**, *25*, 161–166.
- (9) Seeman, P. Targeting the Dopamine D2 Receptor in Schizophrenia. *Expert Opin. Ther. Targets* **2006**, *10*, 515–531.
- (10) Mitsutake, A.; Mori, Y.; Okamoto, Y. Enhanced Sampling Algorithms. *Methods Mol. Biol.* **2013**, *924*, 153–195.
- (11) Cavalli, A.; Spitaleri, A.; Saladino, G.; Gervasio, F. L. Investigating Drug–Target Association and Dissociation Mechanisms Using Metadynamics-Based Algorithms. *Acc. Chem. Res.* **2015**, *48*, 277–285.
- (12) Shukla, D.; Hernandez, C. X.; Weber, J. K.; Pande, V. S. Markov State Models Provide Insights into Dynamic Modulation of Protein Function. *Acc. Chem. Res.* **2015**, *48*, 414–422.
- (13) Grubmüller, H. Predicting Slow Structural Transitions in Macromolecular Systems: Conformational Flooding. *Phys. Rev. E: Stat. Phys., Plasmas, Fluids, Relat. Interdiscip. Top.* **1995**, *52*, 2893–2906.
- (14) Tiwary, P.; Limongelli, V.; Salvalaglio, M.; Parrinello, M. Kinetics of Protein–Ligand Unbinding: Predicting Pathways, Rates, and Rate-Limiting Steps. *Proc. Natl. Acad. Sci. U. S. A.* **2015**, *112*, E386–E391.
- (15) Schmidtke, P.; Luque, F. J.; Murray, J. B.; Barril, X. Shielded Hydrogen Bonds As Structural Determinants of Binding Kinetics: Application in Drug Design. *J. Am. Chem. Soc.* **2011**, *133*, 18903–18910.
- (16) Pearlstein, R. A.; Hu, Q. Y.; Zhou, J.; Yowe, D.; Levell, J.; Dale, B.; Kaushik, V. K.; Daniels, D.; Hanrahan, S.; Sherman, W.; Abel, R. New Hypotheses About the Structure–Function of Proprotein Convertase Subtilisin/Kexin Type 9: Analysis of the Epidermal Growth Factor-Like Repeat A Docking Site Using WaterMap. *Proteins: Struct., Funct., Genet.* **2010**, *78*, 2571–2586.
- (17) Bortolato, A.; Tehan, B. G.; Bodnarchuk, M. S.; Essex, J. W.; Mason, J. S. Water Network Perturbation in Ligand Binding: Adenosine A(2A) Antagonists As a Case Study. *J. Chem. Inf. Model.* **2013**, *53*, 1700–1713.
- (18) Abel, R.; Young, T.; Farid, R.; Berne, B. J.; Friesner, R. A. Role of the Active-Site Solvent in the Thermodynamics of Factor Xa Ligand Binding. *J. Am. Chem. Soc.* **2008**, *130*, 2817–2831.
- (19) Sabbadin, D.; Cianchetta, A.; Moro, S. Perturbation of Fluid Dynamics Properties of Water Molecules During G Protein-Coupled Receptor–Ligand Recognition: the Human A2A Adenosine Receptor As a Key Study. *J. Chem. Inf. Model.* **2014**, *54*, 2846–2855.
- (20) Fleck, B. A.; Hoare, S. R.; Pick, R. R.; Bradbury, M. J.; Grigoriadis, D. E. Binding Kinetics Redefine the Antagonist Pharmacology of the Corticotropin-Releasing Factor Type 1 Receptor. *J. Pharmacol. Exp. Ther.* **2012**, *341*, 518–531.

- (21) Bale, T. L.; Vale, W. W. CRF and CRF Receptors: Role in Stress Responsivity and Other Behaviors. *Annu. Rev. Pharmacol. Toxicol.* **2004**, *44*, 525–557.
- (22) Hemley, C. F.; McCluskey, A.; Keller, P. A. Corticotropin Releasing Hormone—a GPCR Drug Target. *Curr. Drug Targets* **2007**, *8*, 105–115.
- (23) Berman, H. M.; Westbrook, J.; Feng, Z.; Gilliland, G.; Bhat, T. N.; Weissig, H.; Shindyalov, I. N.; Bourne, P. E. The Protein Data Bank. *Nucleic Acids Res.* **2000**, *28*, 235–242.
- (24) Congreve, M.; Andrews, S. P.; Dore, A. S.; Hollenstein, K.; Hurrell, E.; Langmead, C. J.; Mason, J. S.; Ng, I. W.; Tehan, B.; Zhukov, A.; Weir, M.; Marshall, F. H. Discovery of 1,2,4-Triazine Derivatives As Adenosine A(2A) Antagonists Using Structure Based Drug Design. *J. Med. Chem.* **2012**, *55*, 1898–1903.
- (25) Liu, W.; Chun, E.; Thompson, A. A.; Chubukov, P.; Xu, F.; Katritch, V.; Han, G. W.; Roth, C. B.; Heitman, L. H.; IJzerman, A. P.; Cherezov, V.; Stevens, R. C. Structural Basis for Allosteric Regulation of GPCRs by Sodium Ions. *Science* **2012**, *337*, 232–236.
- (26) Jacobson, M. P.; Pincus, D. L.; Rapp, C. S.; Day, T. J.; Honig, B.; Shaw, D. E.; Friesner, R. A. A Hierarchical Approach to All-Atom Protein Loop Prediction. *Proteins: Struct., Funct., Genet.* **2004**, *55*, 351–367.
- (27) Thorsen, T. S.; Matt, R.; Weis, W. I.; Kobilka, B. K. Modified T4 Lysozyme Fusion Proteins Facilitate G Protein-Coupled Receptor Crystallography. *Structure* **2014**, *22*, 1657–1664.
- (28) Friesner, R. A.; Banks, J. L.; Murphy, R. B.; Halgren, T. A.; Klicic, J. J.; Mainz, D. T.; Repasky, M. P.; Knoll, E. H.; Shelley, M.; Perry, J. K.; Shaw, D. E.; Francis, P.; Shenkin, P. S. Glide: a New Approach for Rapid, Accurate Docking and Scoring. 1. Method and Assessment of Docking Accuracy. *J. Med. Chem.* **2004**, *47*, 1739–1749.
- (29) Wootten, D.; Simms, J.; Miller, L. J.; Christopoulos, A.; Sexton, P. M. Polar Transmembrane Interactions Drive Formation of Ligand-Specific and Signal Pathway-Biased Family B G Protein-Coupled Receptor Conformations. *Proc. Natl. Acad. Sci. U. S. A.* **2013**, *110*, 5211–5216.
- (30) Hollenstein, K.; Kean, J.; Bortolato, A.; Cheng, R. K.; Dore, A. S.; Jazayeri, A.; Cooke, R. M.; Weir, M.; Marshall, F. H. Structure of Class B GPCR Corticotropin-Releasing Factor Receptor 1. *Nature* **2013**, *499*, 438–443.
- (31) Schneider, N.; Lange, G.; Hindle, S.; Klein, R.; Rarey, M. A Consistent Description of HYdrogen Bond and DEhydration Energies in Protein-Ligand Complexes: Methods Behind the HYDE Scoring Function. *J. Comput.-Aided Mol. Des.* **2013**, *27*, 15–29.
- (32) Hess, B.; Kutzner, C.; Van Der Spoel, D.; Lindahl, E. GROMACS 4: Algorithms for Highly Efficient, Load-Balanced, and Scalable Molecular Simulation. *J. Chem. Theory Comput.* **2008**, *4*, 435–447.
- (33) Tribello, G. A.; Bonomi, M.; Branduardi, D.; Camilloni, C.; Bussi, G. PLUMED 2: New Feathers for an Old Bird. *Comput. Phys. Commun.* **2014**, *185*, 604–613.
- (34) Dore, A. S.; Bortolato, A.; Hollenstein, K.; Cheng, R. K.; Read, R. J.; Marshall, F. H. Decoding Corticotropin-Releasing Factor Receptor Type 1 Crystal Structure. *Curr. Mol. Pharmacol.* **2015**, submitted.
- (35) Lindorff-Larsen, K.; Piana, S.; Palmo, K.; Maragakis, P.; Klepeis, J. L.; Dror, R. O.; Shaw, D. E. Improved Side-Chain Torsion Potentials for the Amber ff99SB Protein Force Field. *Proteins: Struct., Funct., Genet.* **2010**, *78*, 1950–1958.
- (36) Wang, J.; Wolf, R. M.; Caldwell, J. W.; Kollman, P. A.; Case, D. A. Development and Testing of a General Amber Force Field. *J. Comput. Chem.* **2004**, *25*, 1157–1174.
- (37) Jakalian, A.; Jack, D. B.; Bayly, C. I. Fast, Efficient Generation of High-Quality Atomic Charges. AM1-BCC Model: II. Parameterization and Validation. *J. Comput. Chem.* **2002**, *23*, 1623–1641.
- (38) Jambeck, J. P.; Lyubartsev, A. P. Derivation and Systematic Validation of a Refined All-Atom Force Field for Phosphatidylcholine Lipids. *J. Phys. Chem. B* **2012**, *116*, 3164–3179.
- (39) Wolf, M. G.; Hoefling, M.; Aponte-Santamaria, C.; Grubmüller, H.; Groenhof, G. G\_Membed: Efficient Insertion of a Membrane Protein into an Equilibrated Lipid Bilayer With Minimal Perturbation. *J. Comput. Chem.* **2010**, *31*, 2169–2174.
- (40) Darden, T.; York, D.; Pedersen, L. Particle Mesh Ewald: An N Log (N) Method for Ewald Sums in Large Systems. *J. Chem. Phys.* **1993**, *98*, 10089–10092.
- (41) Bussi, G.; Donadio, D.; Parrinello, M. Canonical Sampling Through Velocity Rescaling. *J. Chem. Phys.* **2007**, *126*, 014101.
- (42) Parrinello, M.; Rahman, A. Polymorphic Transitions in Single Crystals: A New Molecular Dynamics Method. *J. Appl. Phys.* **1981**, *52*, 7182–7190.
- (43) Marchi, M.; Ballone, P. Adiabatic Bias Molecular Dynamics: a Method to Navigate the Conformational Space of Complex Molecular Systems. *J. Chem. Phys.* **1999**, *110*, 3697–3702.
- (44) Barducci, A.; Bussi, G.; Parrinello, M. Well-Tempered Metadynamics: a Smoothly Converging and Tunable Free-Energy Method. *Phys. Rev. Lett.* **2008**, *100*, 020603.
- (45) Branduardi, D.; Gervasio, F. L.; Parrinello, M. From A to B in Free Energy Space. *J. Chem. Phys.* **2007**, *126*, 054103.
- (46) Bolhuis, P. G.; Chandler, D.; Dellago, C.; Geissler, P. L. Transition Path Sampling: Throwing Ropes Over Rough Mountain Passes, in the Dark. *Annu. Rev. Phys. Chem.* **2002**, *53*, 291–318.
- (47) Tiwary, P.; Parrinello, M. From Metadynamics to Dynamics. *Phys. Rev. Lett.* **2013**, *111*, 230602.
- (48) Glossop, P. A.; Watson, C. A.; Price, D. A.; Bunnage, M. E.; Middleton, D. S.; Wood, A.; James, K.; Roberts, D.; Strang, R. S.; Yeadon, M.; Perros-Huguet, C.; Clarke, N. P.; Trevethick, M. A.; Machin, I.; Stuart, E. F.; Evans, S. M.; Harrison, A. C.; Fairman, D. A.; Agoram, B.; Burrows, J. L.; Feeder, N.; Fulton, C. K.; Dillon, B. R.; Entwistle, D. A.; Spence, F. J. Inhalation by Design: Novel Tertiary Amine Muscarinic M(3) Receptor Antagonists With Slow Off-Rate Binding Kinetics for Inhaled Once-Daily Treatment of Chronic Obstructive Pulmonary Disease. *J. Med. Chem.* **2011**, *54*, 6888–6904.